© creative

Scientific paper

Synthesis and Characterization of a Nanosilica-Cysteine Composite for Arsenic(III) Ion Removal

Omar Alnasra* and Fawwaz Khalili

Department of Chemistry, Faculty of Science, The University of Jordan, Amman 11942.

* Corresponding author: E-mail: amr9170169@ju.edu.jo Tel.: +962799413977

Received: 03-26-2023

Abstract

This article describes the synthesis of a nanosilica-cysteine composite (SiO_2 -Cys) and its application as a sorbent and carrier for arsenic(III) using different media. Attenuated total reflectance-Fourier-transform infrared spectroscopy, scanning and transmission electron microscopy, X-ray diffraction, and thermogravimetric analysis were applied to characterize SiO_2 -Cys. Using the batch technique, the sorption of As(III) ions by SiO_2 -Cys was studied, and the effects of pH, sorbent dosage, temperature, initial concentration, and contact time were all taken into consideration. According to kinetic studies, the pseudo-second-order equation adequately described the sorption of the As(III) ion. The spontaneity of the sorption process on SiO_2 -Cys is suggested by the negative values of Gibbs free energy (ΔG°). Positive values of enthalpy (ΔH°) indicate an endothermic adsorption process and positive values of entropy (ΔS°) for the adsorption of As(III) ions mean that adsorption is associated with increasing randomness. The Langmuir model, which has a maximum sorption capacity for SiO_2 -Cys of (66.67 mg/g) at 25 °C, provided a better fit to the sorption isotherm.

Keywords: Arsenic; modification; silica nanoparticles; cysteine; sorption; ion uptake

1. Introduction

Arsenic, a group 15 metalloid element with an atomic weight of 74.9216 amu and atomic number 33, is considered one of the most common elements in nature. 1,2 Arsenic is an element of concern from both an environmental and human health perspective.3 Arsenic is in all its features mostly recognized as a poison. Arsenic species can be found in all kinds of environments and can come from both natural and anthropogenic sources.⁴ The most toxicologically potent arsenic compounds are in the trivalent oxidation state. This is due to their ability to produce reactive oxygen species and their reactivity with compounds that contain sulfur. Nevertheless, humans are exposed to both trivalent and pentavalent arsenicals.⁵ Natural sources of arsenic include weathering, the activity of volcanoes and some biological processes. Anthropogenic sources are diverse from the burning of fossil fuels, smelting, and mining to different types of industrialization (pesticides, desiccants, pigments, and preservatives). However, these are all responsible for the presence of arsenic in water.⁶⁻⁸ The World Health Organization (WHO, Geneva, Switzerland), Environmental Protection Agency (US-EPA, United States)^{9,10} and Central Pollution Control Board (CPCB,

India) 11,12 have established that arsenic in drinking water that is not to exceed a certain level of the range from 0.01 to 0.05 mg L^{-1} due to its extreme toxicity.

Arsenic can be eliminated from aqueous solutions using many physical and chemical treatment methods. Over the past few decades, various techniques have been used, inclusive of sorption, ion exchange, chemical precipitation, and electrodialysis.¹³ Several variables, including the concentration of arsenic, pH, and the interference with competing ions, affect the effectiveness of each of these techniques. Sometimes, they are suitable for As(V), but not for As(III).¹⁴ The efficiency, affordability, and ease of the technique, all play a role in selecting the best arsenic removal method. 15,16 Adsorption is one of the most promising techniques among all those that are currently in use.¹⁷ Moreover, current infrastructure and technologies for treating wastewater and water are at their capacity to provide water of sufficient quality to meet both environmental and human needs. 18,19 Nanoparticles are good options for water treatment applications due to their many diverse properties involving surface area, specificity, and reactivity. 20,21 In the past ten years, reports on the selective and effective adsorption of arsenic ions by silica that have been functionalized with amino

acids,^{22,23} surface ions-imprinted silica,²⁴ or quaternary amines²⁵ have all been made. The purpose of this research is to synthesize composite material using cysteine, where the thiol groups play a major role in the process of As(III) adsorption, and to thoroughly investigate the effectiveness of As(III) removal from water and different media. The main goals are to (a) synthesize and characterize the composite nano-material, (b) to determine the kinetics of As(III) adsorption, and (c) to study the impact of temperature, pH, time, and initial concentration on As(III) adsorption. This is the first novel work that deals with nanosilica-cysteine composite (SiO₂-Cys) and its application as a sorbent and carrier for arsenic(III) using different media.

2. Experimental

2. 1. Materials

Nano powder of SiO₂ (99.5%), L-Cysteine (≥ 98%) from a non-animal source and Luecocrystal violet (4,4′,4″-methylidynetris(N,N-dimethylaniline) from Sigma Aldrich, Ninhydrin from Bio Basic Inc. Hydrochloric acid (37%) from VWR Chemicals, Arsenic trioxide (99.5%) from BDH Chemicals, England. NaOH pellets from Merck.

2. 2. Instruments

The RADWAG® AS 220.R2, Electronic Balance was used for the weighing. A BANTE pH-meter (PHS-25CW) was used to determine the pH of the solutions. The attenuated total reflectance-Fourier transform infrared spectrum was recorded on a Bruker Vertex 70-FT-IR spectrometer at room temperature coupled with a vertex Pt-ATR-FTIR accessory. Centrifugation was done using (DJB Lab Care-AIC PK 130) at 4000 RPM speed. DHP-9052 heating incubator was used to heat the samples. Using a NETZCH STA 409 PG/PC thermal analyzer with a heating rate of 20 °C/min from (0–1000 °C), thermal gravimetric analysis was performed. The Philips X-Pert PW 3060, running at 45 kV and 40 mA, was used to measure X-Ray Diffraction. The 3D shape was examined using a scanning electron microscope NCFL's FEI QUANTA 600 FEG. Shape and size distribution of the nanoparticles were obtained by a Formvar-coated copper grid (Electron Microscopy Sciences, USA) using an FEI Morgagni 268 transmission electron microscopy (Eindhoven, The Netherlands) at a 60 kV accelerating voltage. GRIFFIN (1-150) vacuum oven was used to dry samples at 25 °C and 630 mm Hg. A 1.0 cm quartz cell and a METASH vis-spectrophotometer, model V-5100, were used to measure the As(III) concentration.

2. 3. Modification of Nanosilica with Cysteine

Dissolving 36 g \pm 0.1 mg of the nanosilica powder in 600.0 \pm 0.1 mL of deionized water and adjusting the pH to

 5.60 ± 0.01 . Add 36 g ± 0.1 mg of cysteine to the nanosilica solution and shaking was done using a magnetic stirrer for 48 hrs. Then the mixture was filtered by centrifugation and dried in a vacuum oven at 25 ± 0.5 °C for 5 days (90% yield). The product is labeled as (SiO₂-Cys).

2. 4. Characterization

Attenuated total reflectance-Fourier Transform Infrared (ATR-FTIR) Spectroscopy Analysis

SiO₂-Cys and SiO₂-Cys with As(III) (SiO₂-Cys/ATO) spectra of ATR-FTIR were recorded using a Vertex 70-FT-IR spectrometer (Bruker, Germany) at room temperature coupled with a vertex Pt-ATR-FTIR accessory.

Thermal Gravimetric Analysis (TGA)

The TGA of SiO_2 -Cys and SiO_2 -Cys/ATO was performed using a Netzsch STA 409 PG/PC thermal analyzer (Selb Bavaria, Germany) in the temperature range (0–1000 °C) at a 20 °C/min heating rate and 50 mL/min flow rate for nitrogen purging.

X-ray Diffraction (XRD) Analysis

Philips X pert PW 3060 diffractometer (PANalytical, United Kingdom) was used to investigate the crystalline phases of SiO_2 -Cys and SiO_2 -Cys/ATO. The XRD experiments were operated with Cu K α -radiation (λ = 1.5406 Å) in the 2 θ range (6.0–60.0°) at 45 kV and 40 mA.

Scanning Electron Microscope (SEM)

Information about the surface topography and composition of the sample was examined for SiO₂-Cys and SiO₂-Cys/ATO using NCFL's FEI QUANTA 600 FEG (FEI Ltd, Japan). Disperse 3 mg \pm 0.1 mg of the sample on the carbon tape. Samples weren't further coated before being analyzed.

Transmission Electron Microscopy (TEM)

Shape and size distribution of SiO₂-Cys and SiO₂-Cys/ATO were obtained by a Formvar-coated copper grid (Electron Microscopy Sciences, USA). The grid was left to dry overnight, and a FEI Morgagni 268 TEM (Eindhoven, The Netherlands) was used for imaging (60 kV accelerating voltage).

Point of zero charge (PZC) of SiO₂-Cys

PZC was determined using two methods: Salt Addition and the pH drift method. PZC values by the salt addition method were determined in 0.1 M NaNO $_3$ solution at 25 ± 0.5 °C. In the Salt Addition method, SiO $_2$ -Cys (0.1 g ± 0.1 mg) and 0.1 M NaNO $_3$ (40 ± 0.1 mL) were mixed in different reaction flasks. The pH of the suspension was then adjusted to an initial pH value of 3, 4, 5, 6, 7, 8, 9, 10, and 11 using either 0.1 M HCl or 0.1 M NaOH solutions. Each flask was then vigorously agitated in a shaker for 24 hr. After settling, the final pH of each suspension

was measured very carefully. In the drift method, 0.1 M HCl or 0.1 M NaOH, was used to change the pH of NaNO $_3$ solution to a range of 3 to 11. The pH was measured after SiO $_2$ -Cys (0.1 g \pm 0.1 mg) was added to 20 \pm 0.1 ml of the pH-adjusted solution and equilibrated for 24 hr then the final pH was measured.

2. 5. Removal of As(III) Ions from Water

Preparation of standard curve of As(III)

The stock solution of arsenic (1000 ppm) was prepared by dissolving an appropriate quantity of arsenic trioxide in 20 ± 0.1 mL of 2 ± 0.1 mg g NaOH, which was neutralized by adding dilute HCl to make acid. The solution was then made up to the mark in a 500 mL volumetric flask by adding deionized water. From the stock solution, a working solution of 100 ppm has been prepared. These two solutions were used to build up an analytical calibration curve with various concentrations (0.75, 1.25, 1.50, 2.50, 3.00, 4.00 and 5.00 ppm).

Sorption experiments

Sorption experiments of As(III) implying kinetic studies were conducted in the following simple settings to establish the sorption equilibrium time by SiO_2 -Cys using batch technique; $0.05~g\pm0.1~mg$ of SiO_2 -Cys was shaken with $25.0\pm0.1~mL$ of 50 ppm As(III) ion solution, pH 6 is to be assured, the contact time was varied from 12 to 108 hours at 25.0, 37.5 and 45.0 °C. A spectrophotometric method using Luecocrystal violet indicator to quantify the amount of As(III) ions that were still present in the filtrate was applied. The following equations have been used to calculate the sorption capacity (q_e) and the percentage uptake of As(III) ions:

Uptake (%) =
$$\frac{(C_0 - C_e)}{C_0} \times 100\%$$
 (1)

$$q_e = \frac{(C_0 - C_e)V}{m} \tag{2}$$

where C_0 is the initial As(III) ions concentration (ppm), C_e is the concentration of As(III) ions left in solution at equilibrium, V is the volume (L) of As(III) solution, and m is the mass (g) of SiO₂-Cys.

Sorption isotherms and kinetics modelling

The following two models were used in kinetic evaluation to better understand how As(III) ions adsorb to SiO_2 -Cys:

Pseudo-first-order:

$$\ln(q_e - q_t) = \ln q_e - k_1 t \tag{3}$$

and pseudo-second-order:

$$\frac{t}{q_t} = \frac{1}{k_2 q_e^2} + \frac{t}{q_e} \tag{4}$$

where k_1 , k_2 are the rate constants for pseudo-first-order and pseudo second-order adsorption process, respectively. q_e and q_t (mg/g) are the amounts of As(III) ions adsorbed onto SiO₂-Cys at equilibrium and time t (min).²⁶

The sorption of As(III) ions onto ${\rm SiO_2}$ -Cys was investigated using three different isotherm models: Langmuir, Freundlich, and Dubinin–Radushkevich (D-R). The sorption isotherms were carried out by shaking 0.05 g \pm 0.1 mg of ${\rm SiO_2}$ -Cys with 25.0 \pm 0.1 mL of solutions of variable concentrations (50, 100, 150, 200 and 250 ppm) for As(III) at pH 6.0 \pm 0.01 and at 25.0, 37.5 and 45.0 °C. Samples were shaken for 96 hours, then centrifuged and the amount of As(III) ions left in solution was determined. The adsorption isotherms are studied using the following formulas:

• Langmuir equation (Form I):

$$\frac{C_e}{q_e} = \frac{1}{q_m K_L} + \left(\frac{1}{q_m}\right) C_e \tag{5}$$

• Freundlich equation:

$$Log q_e = \log K_F + \frac{1}{n} \log C_e \tag{6}$$

• Dubinin-Radushkevich equations:

$$\ln q_e = \ln q_{max} - \beta \varepsilon^2 \tag{7}$$

where the Polanyi potential ϵ , can be calculated as:

$$\varepsilon = RT \ln \left(1 + \frac{1}{C_o} \right) \tag{8}$$

Desorption experiments

A 0.05 g \pm 0.1 mg of SiO₂-Cys was dissolved in 25.0 \pm 0.1 mL of 50 ppm As(III) at pH 6.0 \pm 0.01 and 25.0 \pm 0.5 °C, shaken for 96 hours, then centrifuged and dried in a vacuum oven. Adding to vessels containing 50.0 mL media solution (normal saline, dextrose, ringer lactate, water (all at pH = 7.4 \pm 0.01), and 0.1 M HCl, then were shaken at 250 rpm for 48 hr and 37.5 \pm 0.5 °C. After that an aliquot was taken out for the determination of desorbed As(III) ions. The concentration of As(III) in each sample was determined by comparison with a calibration curve based on the absorption maximum at 590 nm.

2. 6. Regeneration and Reusability of SiO₂-Cys

The regeneration and reusability of SiO_2 -Cys after As(III) adsorption/desorption cycles were investigated. Four cycles were performed. 25 \pm 0.1 mL of a 50 ppm As(III) solution at pH 7.4 was contacted with 0.5 g \pm 0.1 mg of SiO_2 -Cys with shaking at 37.5 \pm 0.5 °C during 24 hr. The suspension was centrifuged, the final solution was measured for As(III) content and the remaining solid was washed with 50 \pm 0.1 mL of 0.1 M HCl followed by washing with deionized water. The washed adsorbent was then

dried at 25 ± 0.5 °C in a vacuum oven for 24 hr. The dried solid was weighted, and the process was repeated three more times. The amount of As(III) adsorbed was determined by Equation 2 and the removal % was calculated using Equation 1.

3. Results and Discussion

Nanosilica-cysteine composite (SiO_2 -Cys) was prepared successfully. The yield percentage of the reaction was 90% and a well structural characterization of the synthesized nanoparticles using ATR-FTIR, TGA, SEM, TEM and XRD was achieved.

3. 1. ATR-FTIR Analysis

The ATR-FTIR analysis was performed to establish the changes in the functional groups of SiO₂-Cys to ensure the uptake of As(III). The spectrum of SiO₂-Cys (Figure 1b) shows distinctive peaks at three main wavenumbers: 1077, 800, and 453 cm⁻¹ which corresponds to the asymmetric, symmetric modes of Si-O-Si, bending O-Si-O, respectively, and a characteristic peak at 962 cm⁻¹ for the silanol group stretching vibration.³⁰ The red shift in asymmetric Si-O-Si band from original 1060 cm⁻¹ on nanosilica to 1077 cm⁻¹ on SiO₂-Cys indicated the interaction of amino acid with surface silanols of nanosilica.³¹ Other peaks: 1583 cm⁻¹ (COO⁻ asymmetric stretching), 1486 cm⁻¹ (N-H bending), and 1406 cm⁻¹ (COO⁻ symmetric

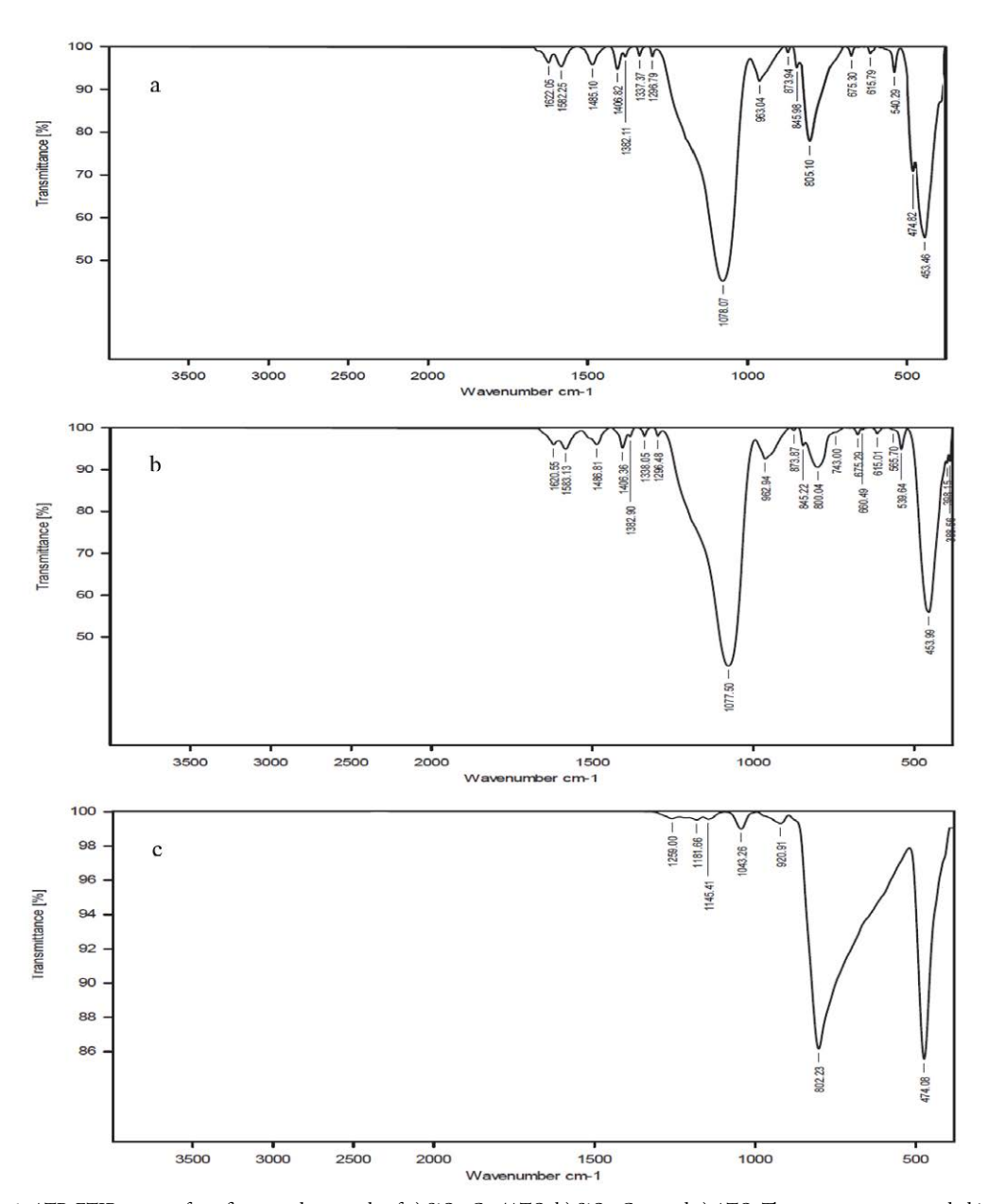


Figure 1. ATR-FTIR spectra for a fine powder sample of a) SiO_2 -Cys/ATO, b) SiO_2 -Cys, and c) ATO. The spectra were recorded in the mid-infrared region (4000–400 cm⁻¹) and show characteristic absorption bands corresponding to the sample's chemical composition and functional groups.

stretching) were also observed. The existence of COO⁻ and N-H peaks showed that cysteine is present as a zwitterion molecule.³²

ATR-FTIR spectra of the bare As_2O_3 (Figure 1c) shows the prominent peak of As–O stretching vibration at 802 cm⁻¹ and another peak at 474 cm⁻¹ which is related to As–O bending.³³

3. 2. TGA Thermogram

The TGA thermogram of SiO₂-Cys in Figure 2 (line 2) consisted of a main gradual weight loss starting at about 180 °C attributed to decomposition loss (about 21 wt %) of the organic component, which is in our case is cysteine. ³⁴ The thermogram showed a prior decomposition occurred around 100 °C, which has to do with the elimination of water that has been adsorbed (physically). ³⁵ TGA thermogram for SiO₂-Cys/ATO which is shown in Figure 2 (line 1) showed two decomposition behaviours; the first

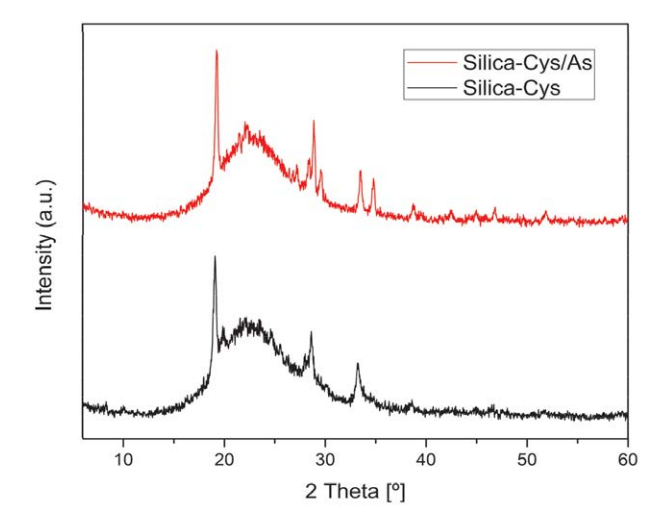


Figure 3. XRD pattern of a sample of SiO₂-Cys and SiO₂-Cys/ATO obtained using a Cu K α radiation source ($\lambda = 1.5406~\text{Å}$) in the 20 range (6.0° – 60.0°).

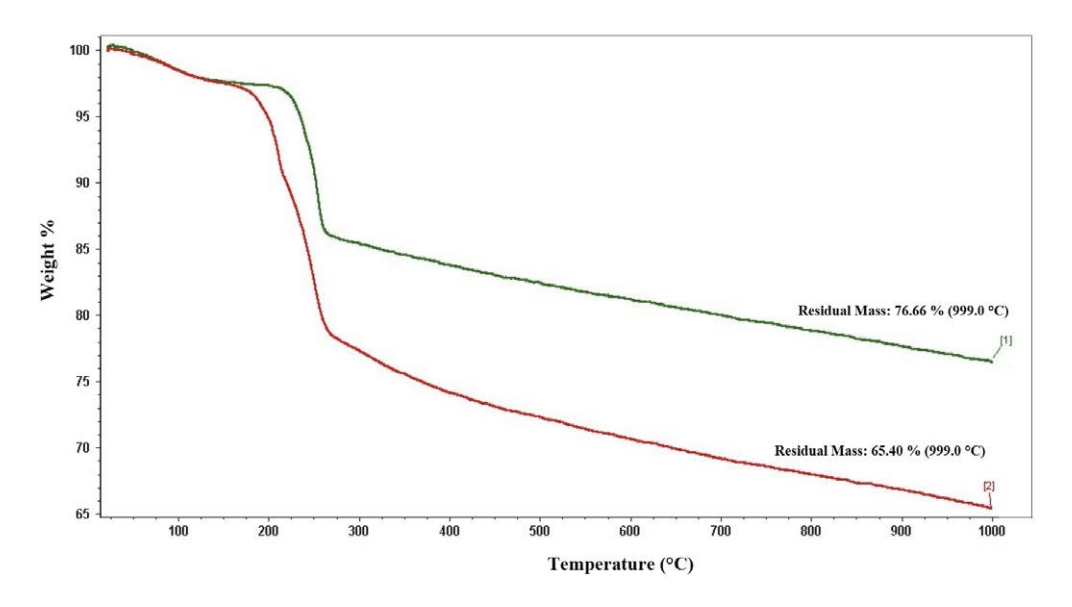


Figure 2. TGA thermogram of [1] SiO_2 -Cys/ATO and [2] SiO_2 -Cys under a nitrogen atmosphere in the temperature range (0–1000 °C). The thermogram shows the weight loss as a function of temperature, revealing the thermal stability and decomposition behavior of the samples.

occurred around 100 °C, which is related to the elimination of water, whereas the second (about 14 wt %) about 220 related to the loss of cysteine. It is obvious from the residual mass percent that SiO₂-Cys/ATO (line 1) retains more mass than SiO₂-Cys (line 2) which can be explained by the existence of the arsenic-oxide in addition to the nanosilica.

3. 3. XRD Pattern

XRD pattern of SiO₂-Cys and SiO₂-Cys/ATO (Figure 3) illustrates important solid-state structural data, represented by the degree of crystallinty. Instead of distinct peaks, a broad hump or diffuse scatter-

ing over a range of angles appeared at $2\theta = 22.50^{\circ}$ for SiO_2 -Cys. This indicates the lack of long-range order characteristic of crystalline materials, this has to be a characteristic peak related to the amorphous silica.³⁶ The presence of three sharp peaks at $2\theta = 19.22^{\circ}$, $2\theta = 28.34^{\circ}$ and $2\theta = 33.46^{\circ}$ associated with the monoclinic crystalline cysteine.³⁷ The XRD pattern of SiO_2 -Cys/ATO possesses two sharp peaks at $2\theta = 29.56^{\circ}$ and $2\theta = 34.78^{\circ}$ corresponding to monoclinic crystal of arsenic trioxide in which the intensity of the peaks indicates the abundance of arsenic trioxide in the sample. Higher peak intensity suggests a higher concentration of ATO.³⁸ This finding confirms the formation of SiO_2 -Cys/ATO.

3. 4. SEM Spectroscopy

Using FEI Quanta SEM, the morphology of SiO₂-Cys and SiO₂-Cys/ATO was examined. All of the SEM

images (Figure 4) showed that the ATO particles had spread out over the SiO₂-Cys system and created a smooth surface.

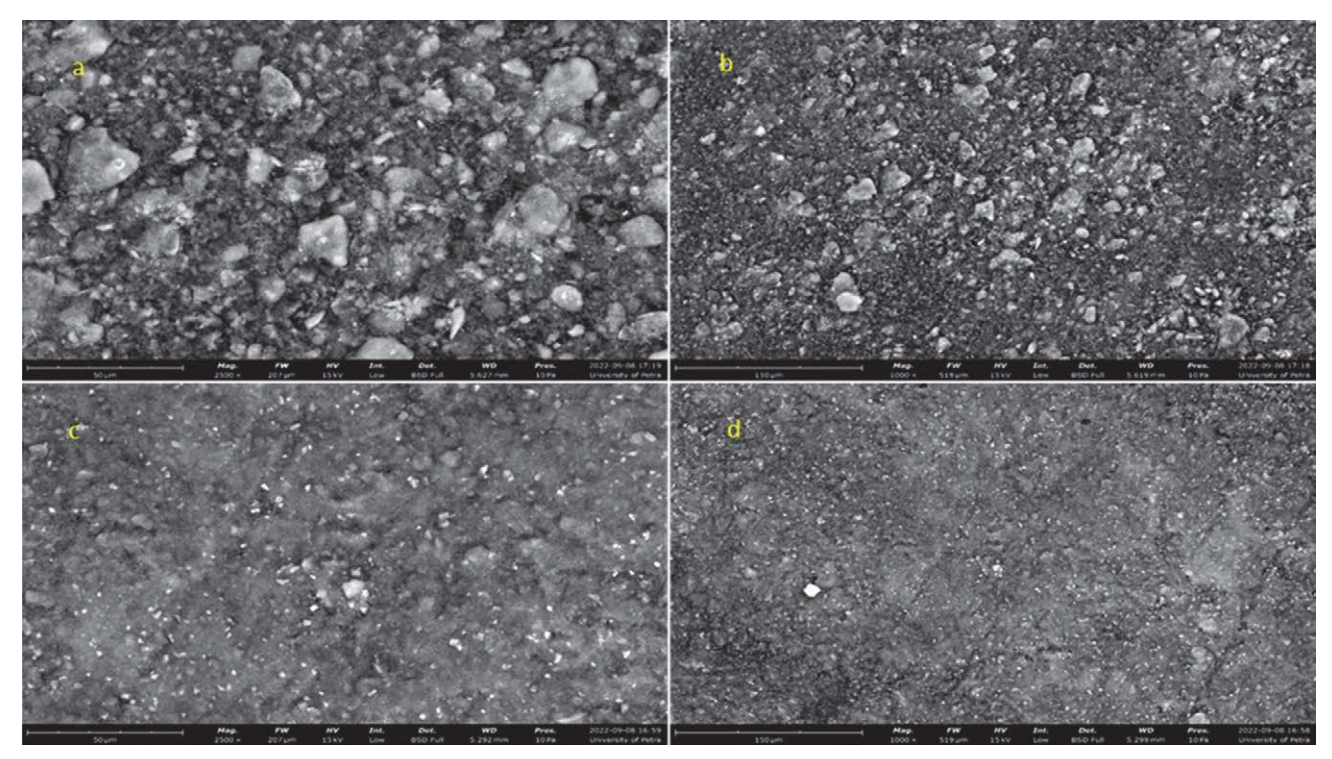


Figure 4. SEM micrographs at different magnifications: (a,c) 2500x-magnification image revealing the surface details and microstructure for SiO₂-Cys and SiO₂-Cys/ATO, respectively. (b,d) 1000x-magnification image showing the overall morphology of SiO₂-Cys and SiO₂-Cys/ATO, respectively.

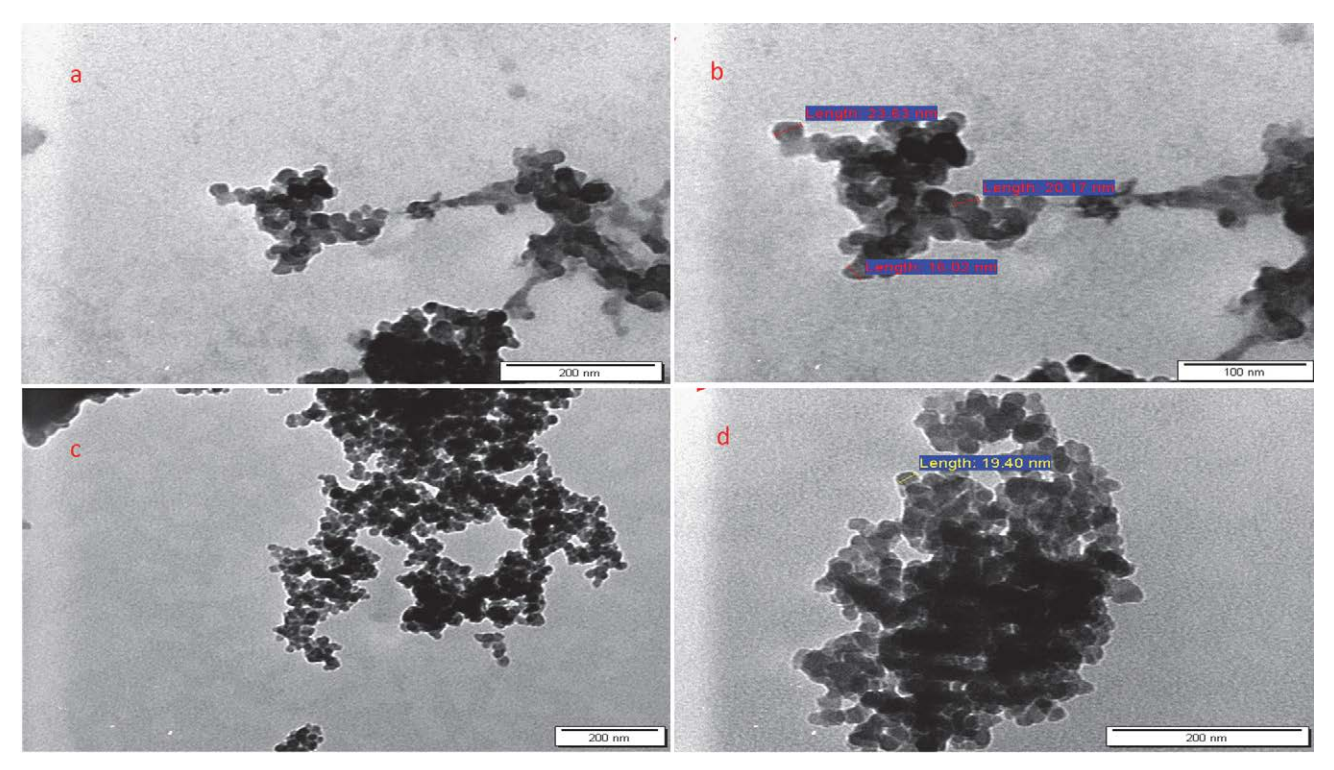


Figure 5. TEM images for (a) SiO_2 -Cys, scale bar: 200 nm (b) SiO_2 -Cys, scale bar: 100 nm; (c,d) SiO_2 -Cys/ATO, scale bar: 200 nm. Images showing the morphology of the samples in the atomic-level.

The adsorption of ATO on nanosilica can involve binding interactions between the ATO molecules and the surface atoms or functional groups of nanosilica (i.e. cysteine). These binding interactions can promote the formation of stable surface species or bridging structures, which can contribute to the smoothness of the surface by reducing surface roughness and promoting surface uniformity. Additionally, ATO adsorption can contribute to surface energy minimization. Adsorbed molecules tend to redistribute and orient themselves to achieve a lower energy state, which can lead to a smoother surface in which the interaction between ATO molecules and the nanosilica surface can facilitate the rearrangement of surface atoms or molecules, reducing height variations and resulting in a more uniform surface.

3. 5. TEM Spectroscopy

TEM analysis was carried out to achieve the shape and size distribution of SiO_2 -Cys and SiO_2 -Cys/ATO. Figure 5 shows that the composite was observed to have dense nano-aggregates possessing a (16–24 nm) particle size and a morphology shape that is roughly spherical in appearance.

Nanosilica particles may have a high surface energy, which can drive them to aggregate and minimize their surface area. Additionally, the presence of ATO can also affect the surface properties of the nanosilica particles,

promoting their aggregation. Surface interactions between the nanosilica and ATO, such as van der Waals forces or chemical bonding, can contribute to the formation of the observed dense nano-aggregates.

3. 6. PZC of SiO₂-Cys

PZC is traditionally known as the pH where one or more components of the surface charge vanishes at a specified temperature, pressure, and aqueous solution composition. PZC was obtained using two methods: Salt Addition and the pH drift method.

PZC values using the salt addition method were determined in 0.1 M NaNO $_3$ solution at 298 K. The pH of the suspension was adjusted to an initial pH value in the range of 3 to 11. The addition of SiO $_2$ -Cys to the NaNO $_3$ solution changes the pH. The final pH values were calculated, and the initial pH values were plotted against Δ pH as seen in Figure 6a. The PZC was chosen to represent the initial pH at which pH is zero. The pH 5 to 11 range, the Δ pH values are positive with a maximum value at pH 10 and the PZC of SiO $_2$ -Cys is pH = 5.

In the drift method, the pH of the 0.01 M NaNO $_3$ was adjusted to a value in the range of 3 to 11. The difference between the final and initial pH was measured and plotted. The PZC was determined to be the pH at which the curve crosses the pH $_{\rm initial}$ = pH $_{\rm final}$ line. 43 The PZC for SiO $_2$ -Cys using the drift method is given in Figure 6b. There are no

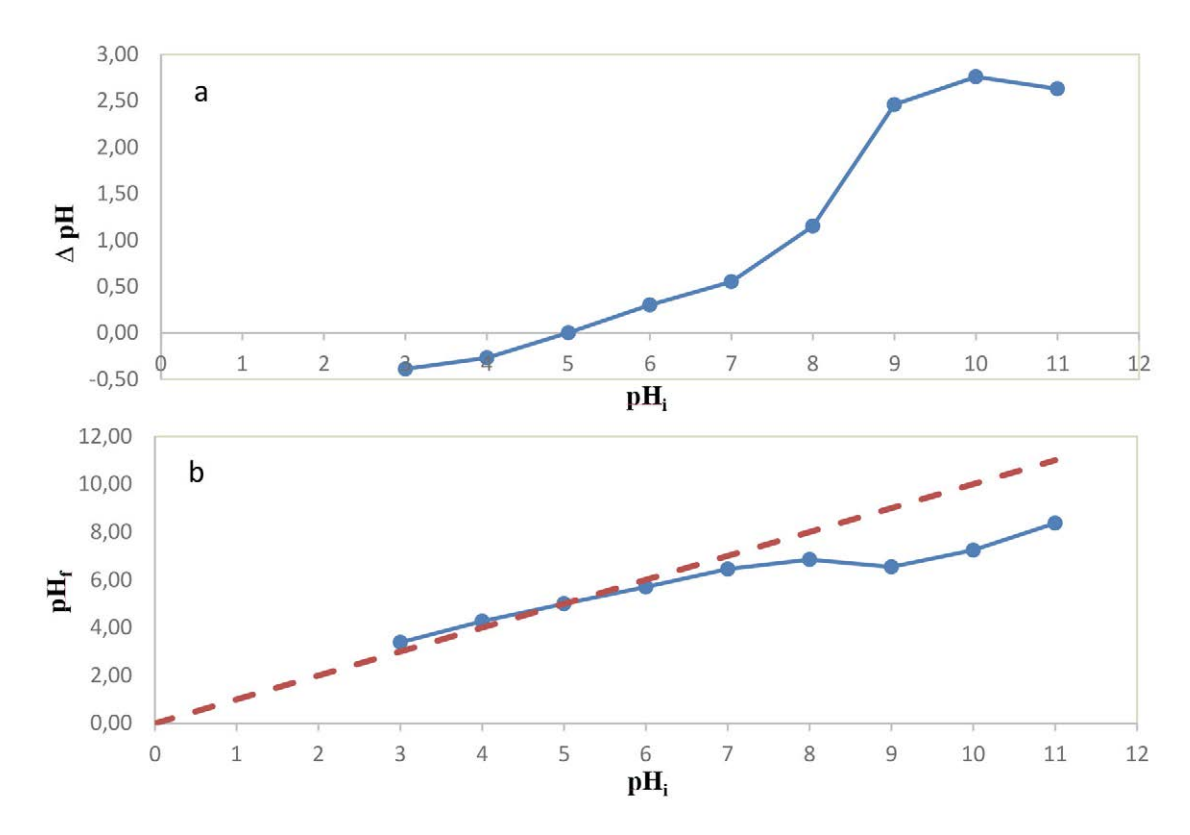


Figure 6. PZC diagram for SiO₂-Cys sample obtained through (a) salt addition method and (b) drift method using 0.1 M NaNO₃ at 25 °C. The diagram illustrates the variation in surface charge as a function of pH, indicating PZC.

ions in the diffuse swarm to neutralize the surface charge at the PZC, so any ions that are adsorbed must be adsorbed in surface complexes.⁴⁰ The PZC achieved (pH = 5), showed the existence of perfect charge balance in the acidic region in an aqueous solution.

3. 7. Effect of Adsorbent Dose

Adsorption capacity reaches a maximum as adsorbent (i.e. SiO₂-Cys) dosage rises, while all other parameters remain constant. As(III) uptake decreases with increasing adsorbent dosage, as shown in Figure 8. Since there are more active sites at lower adsorbent concentrations, increasing the dosage of adsorbent causes particle

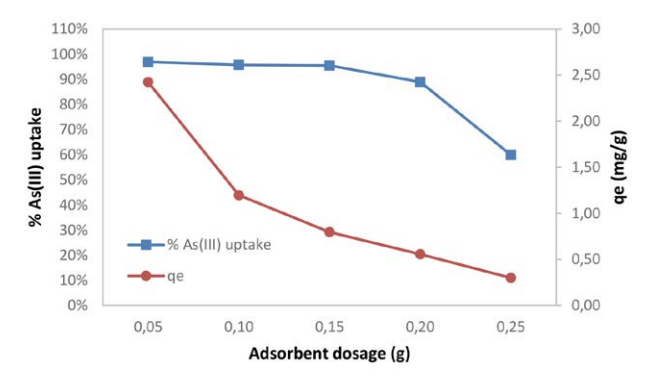


Figure 7. Adsorbent dosage effect on the adsorption of As(III) using SiO_2 -Cys at 25 °C. The graph shows the influence of varying SiO_2 -Cys dosage in the range of 0.05–0.25 g on the adsorption efficiency of As(III).

aggregation, which lowers adsorption capacity and As(III) uptake. Figure 8 shows that 0.05 g of nanosilica has the highest adsorption capacity and achieves a 97% uptake.

3. 8. Effect of pH

Arsenic existing in different forms, alteration in the oxidation state, and solubility in aqueous solutions are all strongly influenced by pH.⁴¹ According to literature,⁴² As(III) species are predominant in nature. Arsenite can be found in water as arsenous acid (H₃AsO₃) with pKa values as shown in Scheme 1.

$$H_3AsO_3 \rightarrow H_2AsO_3^- + H^+ pKa_1 = 9.22$$

 $H_2AsO_3^- \rightarrow HAsO_3^{2-} + H^+ pKa_1 = 12.13$
 $HAsO_3^{2-} \rightarrow AsO_3^{3-} + H^+ pKa_1 = 13.40$

Scheme 1: pKa values of arsenous acid

Arsenic can be soluble in water at pH levels between 2 and 11 with the right chemical and physical conditions, but generally, it is soluble at low pH levels (less than 2).⁴³ Oxidation of the trivalent form of As to pentavalent happens rather slowly; days are needed. Oxidation occurs when air is present between 4 to 9 days. However, it takes 2 to 5 days when pure oxygen is present.⁴⁴

The impact of aqueous solution initial pH values, in the range of pH 3 to 8 on the adsorption behaviour of

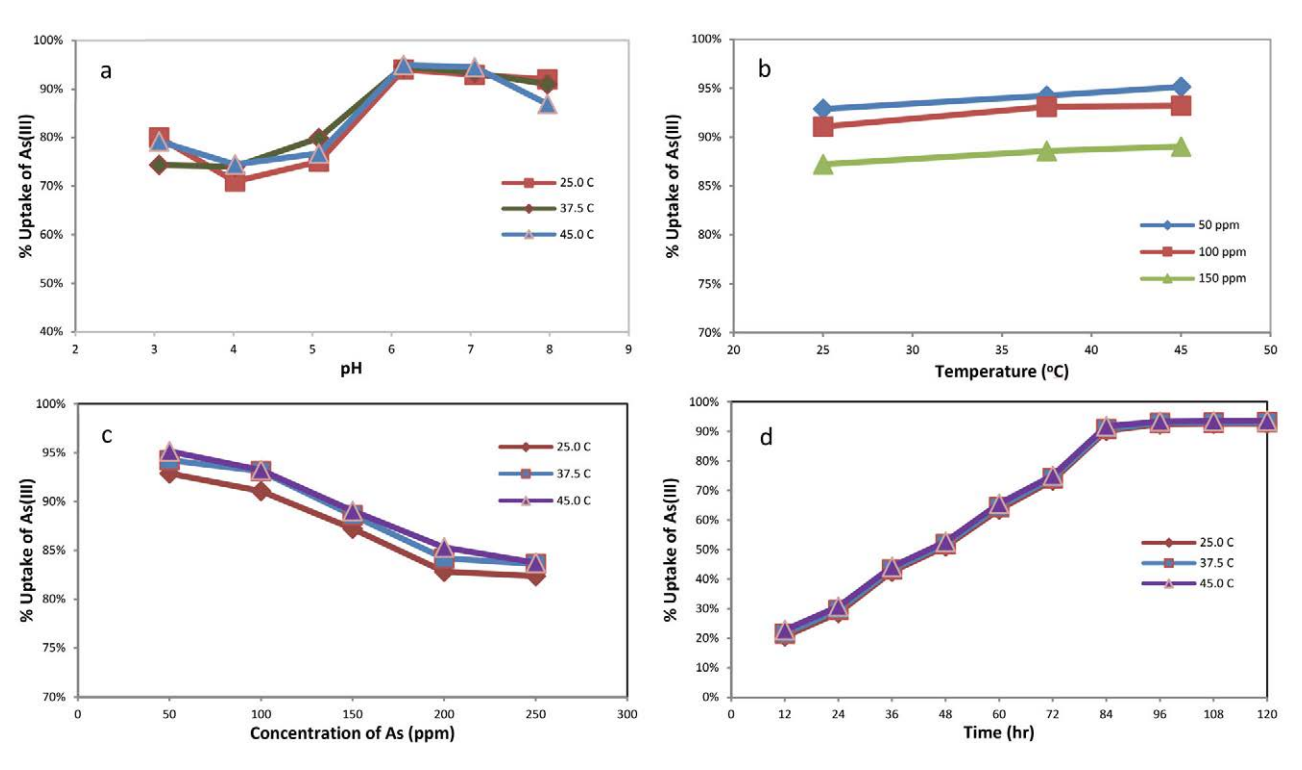


Figure 8. % Uptake of As(III) by 0.05 g of SiO₂-Cys at different (a) pH, (b) temperatures, (c) As(III) concentrations, and (d) contact times. % Uptake experiments were carried out in the range of 25, 37.5, and 45 °C

SiO₂-Cys for fixed As(III) concentration was investigated at different temperatures. It can be clearly observed from Figure 8a that the % uptake of As(III) was low at pH 3 to 5, indicating the existence of competitive adsorption on SiO₂-Cys surface between H₃O⁺ and H₄AsO₃⁺ at low pH, and its approach was constrained by the repulsive force that existed between the protonated surface and H₄AsO₃⁺. After that, the % uptake of As(III) increased from pH 6 to pH 8, where pH 6 produced the highest level of uptake. The positive charges or the negative charges on SiO₂-Cys may change depending on the H⁺ concentration so that H₄AsO₃⁺ ions were more readily absorbed when placed on the silica surface. The percentage of As(I-II) ions that are absorbed increases with increasing solution pH for this reason.⁴⁵ The relation between PZC and the pH of high uptake comes into play when examining the uptake of ions onto a surface. The PZC of a particular surface can be used in the adsorption prediction of an ion onto that surface, with a higher PZC increasing the likelihood of adsorption. To complicate the matter further, the pH of a given solution also impacts ion adsorption. In a basic solution (higher pH) or acidic solution (lower pH), the adsorption of a given ion can be significantly altered or even reduced altogether. So in our case, pH = 5 is the point at which a molecule or surface has neither a net positive nor negative charge, making it a neutral surface, with higher numbers indicating a more basic/ alkaline surface and lower numbers indicating a more acidic surface.

3. 9. Effect of Temperature

For the purpose of determining how temperature affects the adsorption of As(III) by SiO_2 -Cys, experiments were performed at 25, 37.5, and 45 °C. Figure 8b shows a slightly increasing % uptake of As(III) ions as increasing the temperature from 25 to 45 °C, which demonstrated the energy-dependent and endothermic nature of the As(III) ion adsorption mechanism.⁴⁶

3. 10. Effect of Initial Concentration

The initial As(III) concentration was varied from 50 to 250 ppm in order to study the sorption of As(III) ions onto SiO_2 -Cys composite. As(III) ions were readily adsorbed at low initial concentrations of As(III) because there are a lot of adsorption sites available and the surface area is relatively large. As(III) ion removal percentages decline at higher initial concentrations due to a limited number of total adsorption sites (Figure 8c).

3. 11. Contact Time Effect and Models of Sorption Kinetic

It is evident from the findings in Figure 8d that the As(III) ions adsorption efficiency increases rapidly during the first 84 hours before gradually reaching equilibrium. This phenomenon indicates that, with increasing contact time, these binding sites gradually become fewer until reaching saturation, which resulted in decreased uptake and the ad-

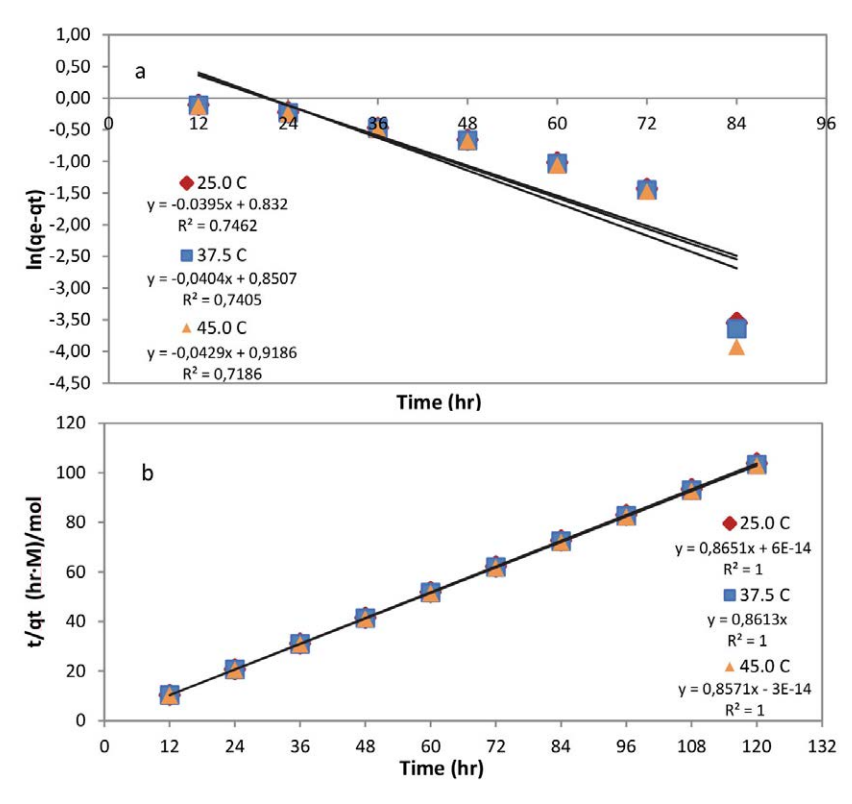


Figure 9. (a) Pseudo-first order and (b) Pseudo-second order adsorption kinetics of 50 ppm As(III) on 0.05 g SiO₂-Cys at pH 6 and different temperatures (25.0, 37.5 and 45.0 °C).

Kinetic models	Parameters	T (K)			
		298	310.5	318	
Pseudo-first-order model	k_1 (L/min)	0.0395	0.0404	0.0429	
	q_e (mg/g)	2.298	2.341	2.506	
	R^2	0.746	0.741	0.719	
Pseudo-second-order model	k_2 (g/mg.min)	0.748	0.742	0.735	
	q_e (mg/g) calculated	1.156	1.161	1.167	
	q_e (mg/g) experimental	1.157	1.163	1.168	
	R^2	1.000	1.000	1.000	

Table 1. Kinetic parameters for adsorption of 50 ppm As(III) on 0.05 g SiO₂-Cys at pH 6 and different temperatures (25.0, 37.5 and 45.0°C).

sorption reaction reaching equilibrium. The equilibrium time has been taken as 96 hours. The linear plots of $[ln(q_e-q_t)$ vs. time] and $[t/q_t$ vs. time] were displayed in Figure 9a and Figure 9b for As(III), and the values of q_e , k_1 , k_2 , and correlation coefficient (R^2) are given in Table 1. The pseudo-second-order kinetic model was better suited to explain the adsorption process of As(III) by SiO₂-Cys due to its R^2 values $(R^2=1.00)$ and its calculated adsorption capacity (q_e) was close to the experimental equilibrium adsorption capacity. One could argue that the rate-controlling step is chemisorption.⁴⁷

3. 12. Initial Concentrations Effect and Models of Sorption Isotherm

To understand what is occurring in the adsorption process (i.e. the mechanism of interaction) we must deal

with adsorption isotherms. Three distinct isotherm models were employed for the adsorption of As(III) onto SiO₂-Cys: Langmuir, Freundlich, and D-R.⁴⁸ Isotherm models as shown in Figures: 10b, 10c and 10d for As(III). Table 2 displays the isotherm parameter values that were determined. The adsorption of As(III) on SiO₂-Cys show high correlation coefficients ($R^2 > 0.97$) for both the Langmuir and Freundlich isotherm models. The fact that the adsorption process included both monolayer and multilayer adsorption possibly contributed to that.

Figure 10a shows the effect of adsorption of the initial concentration of As(III) by SiO_2 -Cys. The adsorption capacities (q_e) of As(III) were obviously increased as the initial concentration of As(III) increased at pH 6. The process of adsorption may have been enhanced because an increase in the initial concentration of As(III) provided a

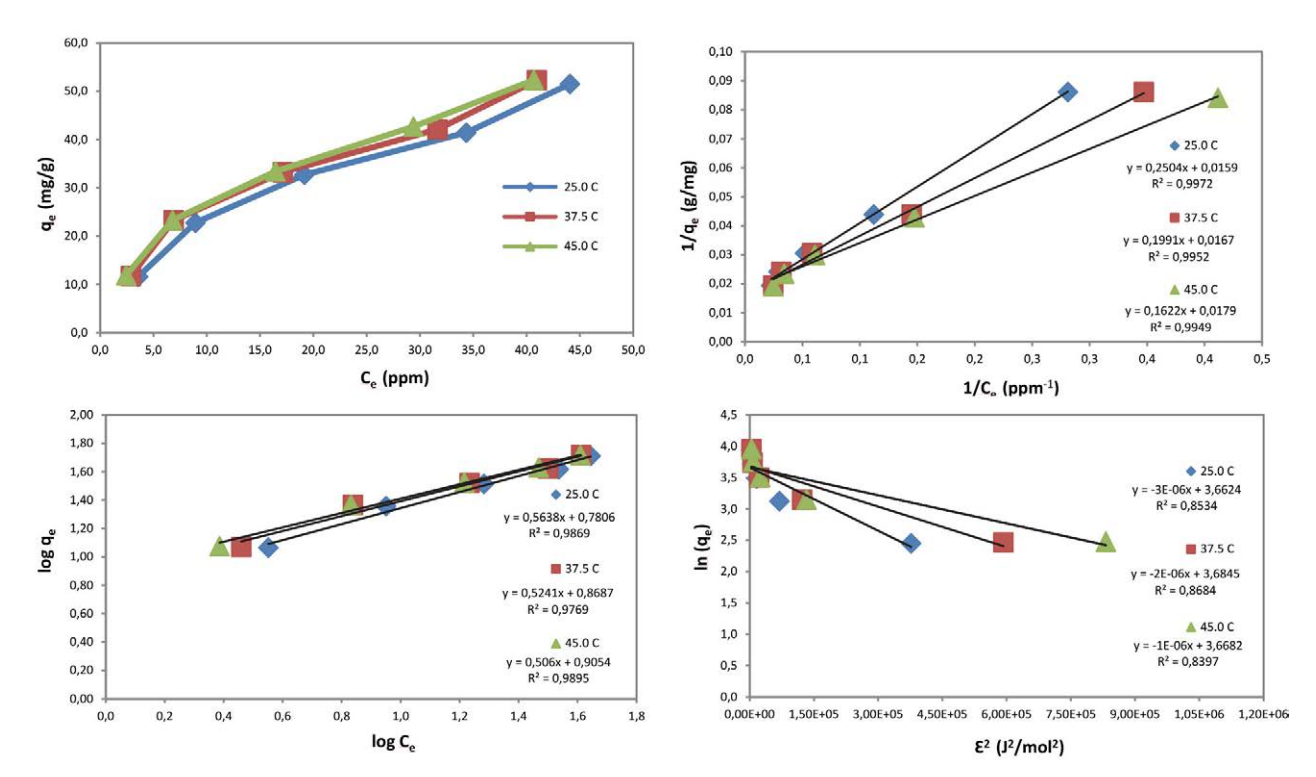


Figure 10. Plots of (a) adsorption isotherm of As(III) on SiO₂-Cys, (b) linearized Langmuir(I), (c) linearized Freundlich, (d) D-R isotherm. The sorption onto $0.05 \, \mathrm{g} \, \mathrm{SiO}_2$ -Cys using the three isotherm models was investigated with solutions of variable concentrations (50, 100, 150, 200 and 250 ppm) for As(III) at pH 6.0 and at 25.0, 37.5 and 45.0 °C.

potent impact to overcome the mass transfer resistance between the solid phase and aqueous phase.⁴⁹

With a finite number of identical centers evenly distributed across the surface of the sorbent, Langmuir adsorption distinguishes monolayer adsorption from other types of adsorption. A high level of adsorption capacity (66.67 mg/g) was attained compared with other sorbents used with As(III) (Table 3). The separation factor (R_L) and also known as the equilibrium parameter can be calculated using the Langmuir isotherm. As shown in Table 2, it was found that (0 < R_L < 1), which can be explained that the adsorption of As(III) on SiO₂-Cys was favourable.⁵⁰ Additionally, despite the unity, which is considered a completely reversible case, the value of R_L tended toward zero (the completely ideal irreversible case).⁵¹

Another model, Freundlich isotherm, is used to describe the adsorption on a solid surface. This model describes heterogeneous surface adsorption. Freundlich constant K_F and n are distinctive features related to the relative sorption capacity of the sorbent and the intensity of sorption, respectively. The values of n, represent the degree of favorability of adsorption. As illustrated in Table 2, the values of n are greater than 1.0, which shows that the adsorption of As(III) on SiO_2 -Cys is a successful process across the entire temperature and concentration range. 52 K_F (mg/g) for the adsorption of As(III) increased with temperature, demonstrating the endothermic nature of the adsorption process. 53

To calculate the apparent free energy of adsorption, the D-R isotherm was used.⁵⁰ This isotherm model is more general than Langmuir isotherm as it rejects the homogenous surface or constant adsorption potential. It is possible to get a good idea of the general mechanism of the sorp-

tion process from the amount of free energy of adsorption (E). Typical values for E range from 8 to 16 kJ/mol, if the adsorption follows ion exchange, and < 8 kJ/mol, if physical adsorption dominates. The calculated E values are reported in Table 2 and indicate that As(III) ion uptake by SiO₂-Cys follows physical adsorption rather than chemical ion exchange.⁵⁴ The same outcomes were observed when examining the values of R_L , K_E , and n.

3. 13. Thermodynamic Studies

The following equations were applied to determine the system's thermodynamic functions, such as changes in Gibbs free energy (ΔG°), enthalpy of adsorption (ΔH°), and entropy of adsorption (ΔS°):

$$\Delta G^{\circ} = -RT \ln K_d = \Delta H^{\circ} - T \Delta S^{\circ} \tag{9}$$

$$lnK_d = \frac{\Delta S^{\circ}}{R} - \frac{\Delta H^{\circ}}{RT} \tag{10}$$

The values of K_d (distribution coefficient) are shown in Table 4, which were calculated from the intercept of $ln(q_e/C_e)$ vs. q_e . Results revealed that K_d rises with T, indicating the endothermic nature⁶³ of As(III) adsorption on SiO₂-Cys.

Table 4. Distribution coefficient for $As(III)\ SiO_2$ -Cys at pH 6.0 at different temperatures.

T (°C)	K_d	lnK_d	
25.0	3.262	1.182	
37.5	4.088	1.408	
45.0	4.895	1.588	

Table 2. Langmuir, Freundlich and D-R isotherm parameters for SiO₂-Cys towards As(III) at different temperatures (25.0, 37.5 and 45.0 °C).

T(°C)	C) Langmuir Isotherm			Fre	Freundlich Isotherm			D-R Isotherm			
	R ²	q_m (mg/g)	K_L (L/mg)	R_{L}	\mathbb{R}^2	n (L/mg)	K_F (mg/g)	R^2	$\frac{B}{(\text{mol}^2/\text{kJ}^2)}$	q_m (mg/g)	E (kJ/mol)
25.0	0.997	66.667	0.060	0.250	0.986	1.776	6.026	0.853	3×10^{-6}	38.939	0.408
37.5	0.995	62.500	0.080	0.199	0.976	1.908	7.379	0.868	2×10^{-6}	39.805	0.500
45.0	0.994	58.824	0.105	0.160	0.989	1.976	8.035	0.839	1×10^{-6}	39.173	0.707

Table 3: Comparison of adsorption capacities of different adsorbents for the removal of As(III)

	Adsorbent	qm (mg/g)	Year of publication	Reference
1	Waste rice husk	0.02	2006	55
2	Non-immobilized sorghum biomass	2.765	2007	56
3	Immobilized sorghum biomass	2.437		
4	Calix arene-appended functional material	0.412	2012	57
5	Thioglycolated sugarcane carbon	0.085	2013	58
6	Fe-Mn binary oxide impregnated chitosan beads	54.2	2015	59
7	Recombinant E. coli expressing arsR	2.32	2018	60
8	Iron-olivine composite	2.831	2018	61
9	Graphene Oxide and Granular Ferric Hydroxide	0.023	2023	62

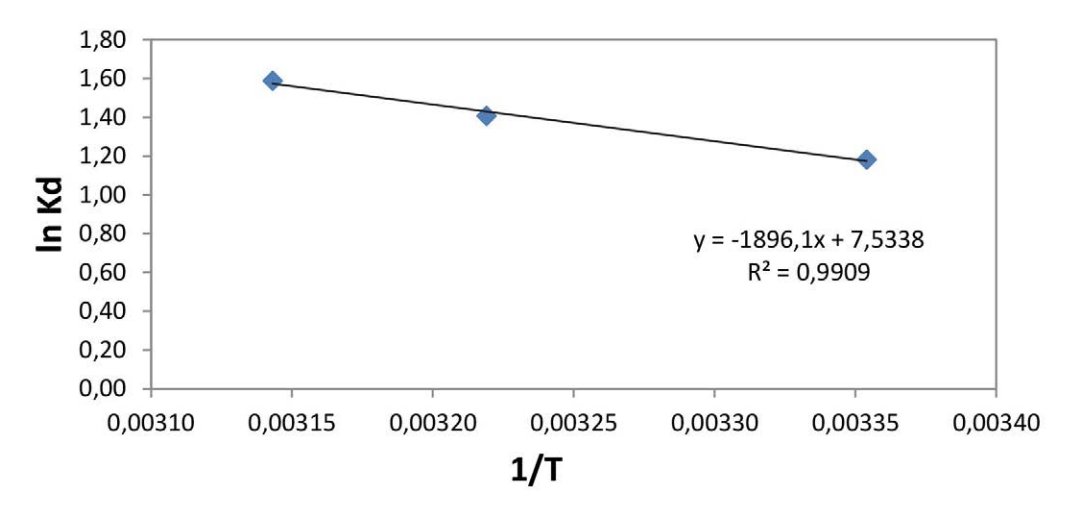


Figure 11. Plot of $ln K_d$ vs 1/T for 50 ppm As(III) on 0.05 g SiO₂-Cys at pH 6.0 and different temperatures (25.0, 37.5 and 45.0°C).

Figure 11 illustrates how ΔH° and ΔS° were determined from the slope and intercept of the plot of $\ln K_d$ vs 1/T for As(III) ion, while ΔG° values were calculated using equation 9.

 ΔG° measures the degree of the spontaneity of the adsorption process. More negative values of the Gibbs free energy represent adsorption processes that are more energetically advantageous.⁶⁴ Results in Table 5 show a negative value of ΔG° , which indicated that the adsorption of As(III) onto SiO₂-Cys is energetically and agreed with K_d values.

Table 5. Thermodynamic parameters for adsorption of As(III) by SiO₂-Cys.

ΔG° (kJ/mol)	ΔH° (kJ/mol)	ΔS° (J/mol K)
-2.931	15.763	62.629

The positive values of ΔH° (Table 5) demonstrated that As(III) on SiO₂-Cys is adsorbed through an endothermic process. In addition, the type of adsorption can be accepted as a physical process when the value of ΔH° is less than 40 kJ/mol.⁶⁵

Van der Waals force and electrostatic force between adsorbate molecules and atoms that make up the adsorbent surface are the main causes of physical adsorption. The As(III) ions are well solvated, so they must lose some of their hydration to be adsorbed, which is one explanation for ΔH° being positive. The energy needed to carry out the ions process of dehydration outweighs the exothermicity of the ions attachment to the surface. ^{54,66}

The increased randomness at the solid/solution interface during the adsorption process is indicated by the positive value of ΔS° for SiO₂-Cys. Adsorbent affinity for the As(III) ions used is also reflected. The presence of randomness in the system is made possible by the fact that

the adsorbed water molecules, which the adsorbate species displace, gain more translational energy than is lost by the adsorbate ions. Dehydration of As(III) ions also makes the system more random.^{66,67}

3. 14. Desorption and Stability Experiments

When dealing with aqueous media solutions, various biological media are options that could be used. The most popular ones were chosen as shown in Table 6. The stability of the sorbent is being compared in these different solutions. Based on the % removal of As(III) by SiO₂-Cys in these solutions, the stability is evaluated. SiO₂-Cys exhibits the highest stability in Ringer lactate, as indicated by the % removal value of 6.22. This suggests that Ringer lactate is effective as a media when delivering As(III) using SiO₂-Cys with a relatively low percentage of the substance released. On the other hand, the sorbent shows the lowest stability in 0.1 M HCl (stomach acidic environment), as indicated by the % removal value of 21.70. This implies that the sorbent is less effective at removing As(III) in 0.1 M HCl compared to other media. A higher percentage of As(III) is released after the sorption process in this solution. Based on these findings, it is concluded that SiO₂-Cys exhibits superior stability and performance in physiological conditions (represented by Ringer lactate), making it more suitable for the desired drug delivery application. It could be further optimized SiO₂-Cys formulation and drug loading process to enhance its stability in physiological environments, ensuring effective drug release and targeted delivery to cancer cells.

3. 15. Regenerability of SiO₂-Cys in Multiple As(III) Adsorption/ Desorption Cycles

The reuse of a functionalized adsorbent is of paramount importance from economic and synthetic points of view. Because of this, the feasibility of reusing SiO_2 -Cys

Media pH		Absorbance of SiO ₂ -Cys*	Absorbance of SiO ₂ -Cys/ATO*	Amount of As(III) detected (ppm)	% Release	
Normal saline	7.4 ± 0.01	0.131	0.361	0.949	18.98	
Dextrose	7.4 ± 0.01	0.102	0.236	0.407	8.14	
Ringer lactate	7.4 ± 0.01	0.102	0.219	0.311	6.22	
Water	7.4 ± 0.01	0.125	0.271	0.475	9.50	
0.1 M HCl	1.0 ± 0.01	0.122	0.376	1.085	21.70	

Table 6. Determination of 5.00 ppm As(III) in presence of nanosilica-cysteine composite from different media at 25 °C

after four reuse cycles was assessed in this work. Results (Figure 12) showed that SiO_2 -Cys loses about 35% of the As(III) removal efficiency in the Ringer lactate media (from ~94% to 58%), about 45% in both the Dextrose and water media, and about 50% in the Normal saline media. These results are encouraging in applying this adsorbent for As(III) in drug delivery and biological systems.

4. Conclusions

The modification of silica nanoparticles with cysteine (SiO₂-Cys) has been carried out and further characterized by ATR-FTIR, TGA, XRD, SEM, and TEM techniques. Using batch sorption experiments under different experimental conditions, the removal of As(III) ions by SiO₂-Cys from aqueous solutions was studied. Was found that the As(III) sorption onto SiO₂-Cys is highly dependent on pH. Kinetic studies indicate that sorption needs 96 hours to reach equilibrium, and its data complied with the pseudo-second-order model well. High correlation coefficients ($R^2 > 0.97$) of the two isotherm models, Langmuir and Freundlich, for the adsorption of As(III) on SiO₂-

Cys are achieved, which can be explained by the fact that both monolayer and multilayer adsorption is included in the process. Thermodynamic parameters demonstrated the endothermic and spontaneous nature of the sorption process.SiO2-Cys represents a featured sorbent in which it works in harmony with the biological environment; this could have a practical application in drug delivery and biological systems (promising candidates for ATO delivery in medical therapy applications). In addition, this sorbent has a high adsorption capacity (66.67 mg/g) and can be reused without significant loss of performance. This characteristic reduces the overall cost and environmental impact associated with using this sorbent. The prepared composite is thus an effective, efficient, and biologically compatible for As(III) adsorption and could be used for ATO delivery in cancer therapy applications.

5. References

- D. R. Lide (Ed.): CRC Handbook of Chemistry and Physics, CRC Press, Boca Raton, Florida, U.S., 2002, pp. 4.4.
- 2. J. A. Dean (Ed.): Lange's Handbook of Chemistry, McGraw-

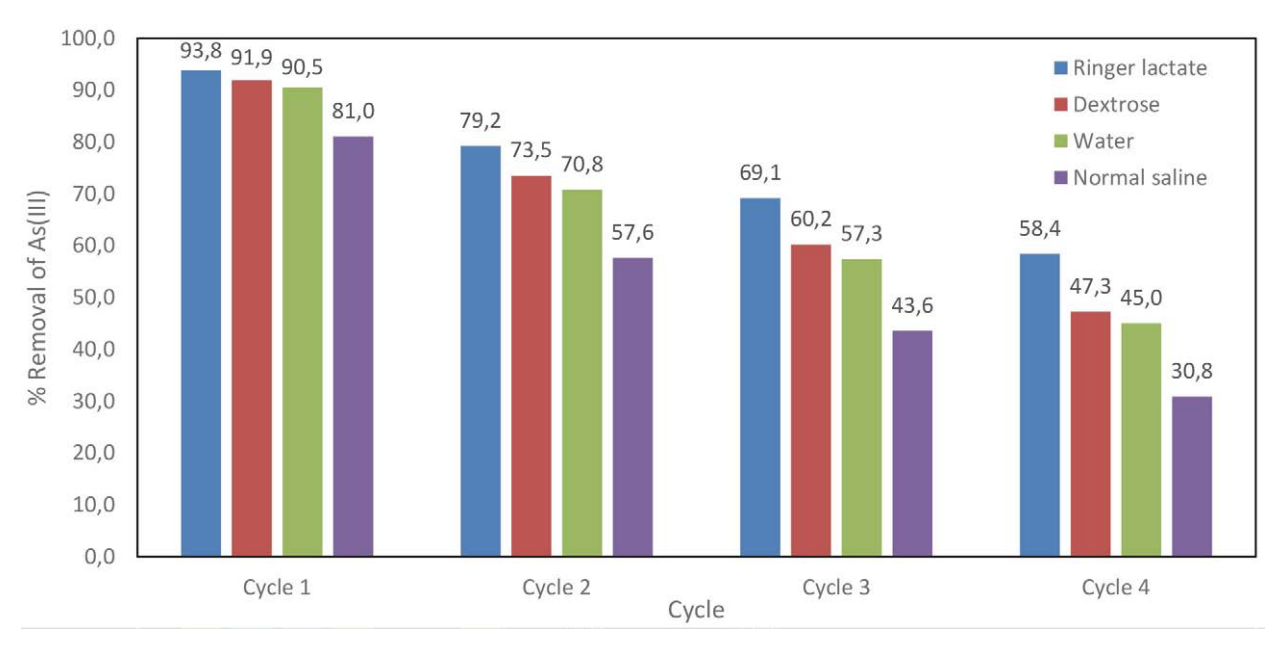


Figure 12. As(III) adsorption/desorption regeneration cycles on SiO₂-Cys, at pH 7.4 and at 37.5°C.

^{*}Mean value of three determinations

- Hill Book Company, New York, U.S., 2002, pp. 3.17.
- 3. J. P. Hughes, L. Polissar, G. Van Belle, Evaluation and synthesis of health effects studies of communities surrounding arsenic producing industries, *Int. J. Epidemiol.* **1988**, *17*, 407–413. **DOI**:10.1093/ije/17.2.407
- 4. National Research Council, *Arsenic in Drinking Water*, The National Academies Press, Washington, DC, U.S., **1999**. pp. 15–16.
- M. F. Hughes, B. D. Beck, Y. Chen, A. S. Lewis, D. J. Thomas, Arsenic Exposure and Toxicology: A Historical Perspective. *Toxicol Sci.* 2011, 123(2), 305–332.
 - DOI:10.1093/toxsci/kfr184
- D. Mohan, P. Charles, Arsenic removal from water/waste-water using adsorbents a critical review, *J. Hazard. Mater.* 2007, 142(1), 1–53. DOI:10.1016/j.jhazmat.2007.01.006
- Y. S. T. Choong, G. T. Chuah, H.Y Robia, L. F. G. Koay, I. Azni, Arsenic toxicity, health hazards and removal techniques from water: an overview, *Desalination* 2007, 217, 139–166.
 DOI:10.1016/j.desal.2007.01.015
- S. Shevade, R. Ford, Use of synthetic zeolites for arsenate removal from pollutant water, *Water Res.* 2004, 38, 3197–3204.
 DOI:10.1016/j.watres.2004.04.026
- 9. WHO, *Exposure to arsenic: a major public health concern*, WHO Document Production Services, Geneva, Switzerland, **2010**, pp. 1–3.
- EPA, Environmental Pollution Control Alternatives, EPA/625/ 5-90/025, EPA/625/4-89/023, Cincinnati, US, 1990, pp.19.
- M. J. Maushkar, Guidelines for water quality monitoring, Central pollution control board (A Government of India organisation), Delhi, India, 2007.
- 12. BIS, *Indian Standard Drinking Water Specification*, Bureau of Indian Standard Publication, New Delhi, India, **1991**, pp. 3.
- 13. T. R. Harper, N. W. Kingham, Removal of arsenic from wastewater using chemical precipitation methods, *Water Environ. Res.* **1992**, *64*, 200. **DOI:**10.2175/WER.64.3.2
- 14. W. H. Ficklin, Separation of arsenic(III) and arsenic(V) in ground waters by ion-exchange, Talanta. **1983**, *30*, 371. **DOI:**10.1016/0039-9140(83)80084-8
- D. Mohan, C.U. Pittman, Arsenic Removal from Water/ Wastewater Using Adsorbents-A Critical Review, *J. Hazard.* Mater. 2007, 142, 1–53. DOI:10.1016/j.jhazmat.2007.01.006
- A. B. Mukherjee, P. Bhattacharya, Arsenic in groundwater in the Bengal Delta Plain: slow poisoning in Bangladesh, *Environ. Rev.* 2001, 9(3), 189–220. DOI:10.1139/a01-007
- S. W. Wan Ngah, C. L. Teong, M.K. Hanafiah, Adsorption of dyes and heavy metal ions by chitosan composites a review, *Carbohydr. Polym.* 2011, 83, 1446–1456.
 - DOI:10.1016/j.carbpol.2010.11.004
- P. Pillewan, S. Mukherjee, T. Roychowdhury, S. Das, A. Bansiwal, S. Rayalu, Removal of As(III) and As(V) from water by copper oxide incorporated mesoporous alumina, *J. Hazard. Mater.* 2011, 186, 367–375.
 - DOI:10.1016/j.jhazmat.2010.11.008
- 19. X. Qu, P. Alvarez, Q. Li, Applications of nanotechnology in water and wastewater treatment, *Water Res.* **2013**, *47*, 3931–3946. **DOI:**10.1016/j.watres.2012.09.058

- 20. K. Hristovski, A. Baumgardner, P. Westerhoff, Selecting metal oxide nanomaterials for arsenic removal in fixed bed columns: from nanopowders to aggregated nanoparticles media, *J. Hazard. Mater.* 2007, 147(1), 265–274.
 DOI:10.1016/j.jhazmat.2007.01.017
- X. Qu, J. Brame, Q. Li, P. Alvarez, Nanotechnology for a safe and sustainable water supply: enabling integrated water treatment and reuse, *Acc. Chem. Res.* 2013, 46(3), 834–843.
 DOI:10.1021/ar300029v
- 22. M. S. Angotzi, V. Mameli, C. Cara, K. B. Borchert, C. Steinbach, R. Boldt, D. Schwarz, C. Cannas, Meso- and Macroporous Silica-Based Arsenic Adsorbents: Effect of Pore Size, Nature of the Active Phase, and Silicon Release. *Nanoscale Adv.* 2021, 3, 6100–6113. DOI:10.1039/D1NA00487E
- 23. J. Dobrynska, Amine- and Thiol-Functionalized SBA-15: Potential Materials for As(V), Cr(VI) And Se(VI) Removal from Water. Comparative Study, *J. Water Proc. Eng.* **2021**, *40*, 101942. **DOI**:10.1016/j.jwpe.2021.101942
- 24. H. T. Fan, X. Fan, J. Li, M. Guo, D. Zhang, F. Yan, T. Sun, Selective Removal of Arsenic(V) from Aqueous Solution Using a Surface-Ion Imprinted Amine-Functionalized Silica Gel Sorbent, *Ind. Eng. Chem. Res.* 2012, 51, 5216–5223. DOI:10.1021/ie202655x
- O. Valdés, A. Marican, Y. Mirabal-Gallardo, L.S. Santos, Selective and Efficient Arsenic Recovery From Water Through Quaternary Amino-Functionalized Silica, *Polymers (Basel, Switz.)* 2018, 10, 626. DOI:10.3390/polym10060626
- S. Azizian, Kinetic models of sorption: a theoretical analysis,
 J. Colloid Interface Sci. 2004, 276, 47–52.
 DOI:10.1016/j.jcis.2004.03.048
- 27. Langmuir, The sorption of gases on plane surfaces of glass, mica and platinum, *J. Am. Chem. Soc.* **1918**, *40*, 1361–1403. **DOI:**10.1021/ja02242a004
- 28. H. Freundlich, Over the sorption in solution, *J. Phys. Chem.* **1906**, *57*, 385–470. **DOI**:10.4236/ajac.2013.47A001
- 29. M.M. Dubinin, L.V. Radushkevich, Equation of the characteristic curve of activated charcoal, *Chem. Zentralbl.* **1947**, *1*, 875–890.
- 30. T. Fan, Y. Liu, B. Feng, G. Zeng, C. Yang, M. Zhou, H. Zhou, X. Wang, Biosorption of cadmium(II), zinc(II) and lead(II) by Penicillium simplicissimum: Isotherms, kinetics and thermodynamics, *J. Hazard. Mater.* **2008**, *160*(2), 655–661. **DOI:**10.1016/j.jhazmat.2008.03.038
- M. Du, Y. Zheng, Modification of silica nanoparticles and their application in UDMA dental polymeric composites, *Polym. Compos.* 2007, 28, 198–207. DOI:10.1002/pc.20377
- 32. A. Khataee, A. Movafeghi, F. Nazari, F. Vafaei, M. Dadpour, Y. Hanifehpour, S. Joo, The toxic effects of L-Cysteine-capped cadmium sulfide nanoparticles on the aquatic plant Spirodela polyrrhiza, *J. Nanopart. Res.* **2014**, *16*, 2774–2784. **DOI:**10.1007/s11051-014-2774-7
- 33. V. Jadhav, S. Sachar, S. Chandra, D. Bahadur, P. Bhatt, Synthesis and Characterization of Arsenic Trioxide Nanoparticles and Their In Vitro Cytotoxicity Studies on Mouse Fibroblast and Prostate Cancer Cell Lines, *J. Nanosci. Nanotechnol.* 2016, 16, 7599–7605. DOI:10.1166/jnn.2016.11663

- 34. I. M. Weiss, C. Muth, R. Drumm, H. Kirchner, Thermal decomposition of the amino acids glycine, cysteine, aspartic acid, asparagine, glutamic acid, glutamine, arginine and histidine, *BMC Biophysics*. **2018**, *11*(1), 1–15.
 - DOI:10.1186/s13628-018-0042-4
- 35. J. Wu, G. Ma, P. Li, L. Ling, B. Wang, Surface modification of nanosilica with acrylsilane-containing tertiary amine structure and their effect on the properties of UV curable coating, *J. Coat. Technol. Res.* 2014, 11(3), 387–395.
 - DOI:10.1007/s11998-013-9552-9
- V. Jafari, A. Allahverdi, Synthesis and Characterization of Colloidal Nanosilica via an Ultrasound Assisted Route Based on Alkali Leaching of Silica Fume, *Int. J. Nanosci. Nanotech*nol. 2014, 10(3), 145–152.
- 37. H. Chen, H. Bian, J. Li, X. Guo, X. Wen, J. Zheng, Molecular Conformations of Crystalline L-Cysteine Determined with Vibrational Cross Angle Measurements, *J. Phys. Chem. B.* **2013**, *117*, 15614–15624. **DOI:**10.1021/jp406232k
- 38. H. Longa, X. Huanga, Y. Zhenga, Y. Pengb, H. He, Purification of crude As₂O₃ recovered from antimony smelting arsenic-alkali residue, *Process Saf. Environ. Prot.* **2020**, *139*, 201–209. **DOI:**10.1016/j.psep.2020.04.015
- 39. T. Mahmood, M.T. Saddique, A. Naeem, P. Westerhoff, S. Mustafa, A. Alum, Comparison of Different Methods for the Point of Zero Charge Determination of NiO, *Ind. Eng. Chem. Res.* 2011, 50, 10017–10023. DOI:10.1021/ie200271d
- 40. M. Khan, A. Sarwar, Determination of Points of Zero Charge of Natural and Treated Adsorbents, *Surf. Rev. Lett.* **2007**, 14(3), 461–469. **DOI:**10.1142/S0218625X07009517
- W.R. Cullen, K.J. Reimer, Arsenic speciation in the environment, *Chem. Rev.* 1989, 89, 713–764.
 DOI:10.1021/cr00094a002
- L. Rajakovic, V. Rajakovic-Ognjanovic (Ed.): Arsenic in Water: Determination and Removal in Arsenic - Analytical and Toxicological Studies, InTech, 2018. DOI: 10.5772/intechopen.72058. DOI:10.5772/intechopen.72058
- H. Garelick, A. Dybowska, E. Valsami-Jones, N. Priest, Remediation Technologies for Arsenic Contaminated Drinking Waters, *J. Soils Sediments.* 2005, 5, 182–190.
 DOI:10.1065/jss2005.06.140
- 44. P. Jana, REMOVAL OF ARSENIC(III) FROM WATER WITH A NEW SOLID-SUPPORTED THIOL, College of Arts and Sciences, University of Kentucky, Lexington, Kentucky, 2012.
- F. Khalili, A. Khalifa, G. Al-Banna, Removal of uranium(-VI) and thorium(IV) by insolubilized humic acid originated from Azraq soil in Jordan, *J. Radioanal. Nucl. Chem.* 2017, 311, 1375–1392. DOI:10.1007/s10967-016-5031-y
- 46. Y. Huang, Y. Hu, L. Chen, T. Yang, H. Huang, R. Shi, P. Lu, C. Zhong, Selective biosorption of thorium (IV) from aqueous solutions by ginkgo leaf, *PLOS ONE*. 2018, *13*(3), 0193659. DOI:10.1371/journal.pone.0193659
- L. Dolatyari, M. Yaftian, S. Rostamnia, Removal of uranium(-VI) ions from aqueous solutions using Schiff base functional-ized SBA-15 mesoporous silica materials, *J. Environ. Manage.* 2016, 169, 8–17. DOI:10.1016/j.jenvman.2015.12.005
- 48. K. Foo, B. Hameed, Insights into the modeling of adsorption

- isotherm systems, *Chem. Eng.* J. **2010**, *156*, 2–10. **DOI**:10.1016/j.cej.2009.09.013
- 49. Z. Naseem, H. Bhatti, S. Sadaf, S. Noreen, S. Ilyas, Sorption of uranium (VI) by Trapa bispinosa from aqueous solution, effect of pretreatments and modeling studies, *Desalin. Water Treat.* **2016**, *57*(24), 11121–11132.
 - DOI:10.1080/19443994.2015.1041059
- D. Humelnicu, C. Blegescu, D. Ganju, Removal of uranium(-VI) and thorium(IV) ions from aqueous solutions by functionalized silica: kinetic and thermodynamic studies, *J. Radioanal. Nucl. Chem.* 2014, 299, 1183–1190.
 - DOI:10.1007/s10967-013-2873-4
- 51. E. Prasetyo, Synthesis of a humic acid-silica gel as a low cost adsorbent for uranium and thorium removal from wastewater, Division of Environmental Science Development, Graduate School of Environmental Science, Hokkaido University, **2016**, pp. 91–92.
- 52. S. Chegrouche, A. Mellah, M. Barkat, A. Aknoun, Kinetics and Isotherms for Uranium (VI) Adsorption from Aqueous Solutions by Goethite, *Am. J. Mater. Sci.* **2016**, *3*(2), 6–12.
- 53. U.H. Kaynar, M. Ayvacıklı, U. Hiçsönmez, S.C. Kaynar, Removal of thorium(IV) ions from aqueous solution by a novel nanoporous ZnO: isotherms, kinetic and thermodynamic studies, *J. Environ. Radioact.* **2015**, *150*, 145–151. **DOI:**10.1016/j.jenvrad.2015.08.014
- 54. A.S. Singha, A. Guleria, Chemical modification of cellulosic biopolymer and its use in removal of heavy metal ions from wastewater, *Int. J. Biol. Macromol.* **2014**, *67*, 409-417. **DOI:**10.1016/j.ijbiomac.2014.03.046
- 55. M. Amin, S. Kaneco, T. Kitagawa, A. Begum, H. Katsumata, T. Suzuki, K. Ohta, Removal of arsenic in aqueous solutions by adsorption onto waste rice husk, *Ind. Eng. Chem. Res.* 2006, 45, 8105–8110. DOI:10.1021/ie060344j
- N. Haque, G. Morrison, G. Perrusquia, M. Gutierrez, A. Aguilera, I. Cano-Aguilera, J. Gardea-Torresdey, Characteristics of arsenic adsorption to sorghum biomass, *J. Hazard. Mater.* 2007, 145, 30–35. DOI:10.1016/j.jhazmat.2006.10.080
- I. Qureshi, S. Memon, Synthesis and application of calixarenebased functional material for arsenic removal from water, Appl. Water Sci. 2012, 2, 177–186.
 DOI:10.1007/s13201-012-0035-4
- 58. P. Roy, N. Mondal, S. Bhattacharya, B. Das, K. Das, Removal of arsenic(III) and arsenic(V) on chemically modified low-cost adsorbent: batch and column operations, *Appl. Water Sci.* **2013**, *3*, 293–309. **DOI:**10.1007/s13201-013-0082-5
- 59. J. Qi, G. Zhang, H. Li, Efficient removal of arsenic from water using a granular adsorbent: Fe-Mn binary oxide impregnated chitosan bead, *Bioresour. Technol.* **2015**, *193*, 243–249. **DOI:**10.1016/j.biortech.2015.06.102
- 60. C. Ke, C. Zhao, C. Rensing, S. Yang, Y. Zhang, Characterization of recombinant E. coli expressing arsR from Rhodopseudomonas palustris CGA009 that displays highly selective arsenic adsorption, *Appl. Microbiol. Biotechnol.* 2018, 102, 6247–6255. DOI:10.1016/j.jenvman.2017.12.040
- P. Ghosal, K. Kattil, M. Yadav, A. Gupta, Adsorptive removal of arsenic by novel iron/olivine composite: Insights into prepa-

- ration and adsorption process by response surface methodology and artificial neural network, *J. Environ. Manage.* **2018**, 209, 176–187. **DOI:**10.1016/j.jenvman.2017.12.040
- 62. A. Tolkou, E. Rada, V. Torretta, M. Xanthopoulou, G. Kyzas, I. Katsoyiannis, Removal of Arsenic(III) from Water with a Combination of Graphene Oxide (GO) and Granular Ferric Hydroxide (GFH) at the Optimum Molecular Ratio, C. 2023, 9, 10. DOI:10.3390/c9010010
- 63. T. Sato, S. Motomura, Y. Ohno, Adsorption and desorption of metal ions by systems based on cellulose derivatives that contain amino acid residues, Textile Society Journal. 1985, 41 (6), 235–240. DOI:10.2115/fiber.41.6_T235
- L. Xia, K. Tan, X. Wang, W. Zheng, W. Liu, C. Deng, Uranium Removal from Aqueous Solution by Banyan Leaves: Equilibrium, Thermodynamic, Kinetic, and Mechanism Studies, *J. Env. Engin.* 2013, 139, 887-895.

- DOI:10.1061/(ASCE)EE.1943-7870.0000695
- Z. Talip, M. Eral, U. Hicsonmez, Adsorption of thorium from aqueous solutions by perlite, *J. Environ. Radioact.* 2009, 100, 139–143. DOI:10.1016/j.jenvrad.2008.09.004
- 66. G. Mirzabe, A. Keshtkar, Selective sorption of U(VI) from aqueous solutions using a novel aminated Fe₃O₄@SiO₂/PVA nanofiber adsorbent prepared by electrospinning method, *J. Radioanal. Nucl. Chem.* 2015, 303(1), 561–576.
 DOI:10.1007/s10967-014-3478-2
- 67. F. Khalili, G. Al-Banna, Adsorption of uranium(VI) and thorium(IV) by insolubilized humic acid from Ajloun soil Jordan, *J. Environ. Radioact.* 2015, 146, 16–26.
 DOI:10.1016/j.jenvrad.2015.03.035

Povzetek

Ta članek opisuje sintezo nanosilicijevega dioksida in cisteinskega kompozita (SiO₂-Cys) ter njegovo uporabo kot sorbenta in nosilca za arzen(III) z uporabo različnih medijev. Za karakterizacijo SiO₂-Cys so uporabili infrardečo spektroskopijo oslabljene popolne odbojnosti s Fourierovo transformacijo, vrstično in transmisijsko elektronsko mikroskopijo, rentgensko difrakcijo in termogravimetrično analizo. S šaržno tehniko smo proučevali sorpcijo As(III) iona s SiO₂-Cys, pri čemer smo upoštevali vplive pH, odmerka sorbenta, temperature, začetne koncentracije in kontaktnega časa. Glede na kinetične študije je enačba psevdodrugega reda ustrezno opisala sorpcijo iona As(III). Na spontanost sorpcijskega procesa na SiO₂-Cys nakazujejo negativne vrednosti Gibbsove proste energije (ΔG°). Pozitivne vrednosti entalpije (ΔH°) kažejo na endotermni proces adsorpcije, pozitivne vrednosti entropije (ΔS°) za adsorpcijo ionov As(III) pa pomenijo, da je adsorpcija povezana z naraščajočo naključnostjo. Langmuirjev model, ki ima največjo sorpcijsko kapaciteto za SiO₂-Cys (66,67 mg/g) pri 25 °C, je zagotovil boljše prileganje sorpcijski izotermi.



Except when otherwise noted, articles in this journal are published under the terms and conditions of the Creative Commons Attribution 4.0 International License